

Large-eddy simulation of flow over a circular cylinder

W. Cheng^{1,2}, D.I. Pullin², R. Samtaney¹, W. Zhang¹ and W. Gao¹

¹ Mechanical Engineering, King Abdullah University of Science and Technology, 4700 KAUST, Thuwal 23955-6900, Saudi Arabia

² Graduate Aerospace Laboratories, California Institute of Technology, Pasadena, CA, 91125

Abstract

We present wall-resolved large-eddy simulation of flow over cylinder up to $Re_D = 10^5$, based on the cylinder diameter D , in the subcritical regime. The numerical method is fourth-order finite-difference on a standard curvilinear O-grid. The stretched-vortex sub-grid scale model is used in the whole domain, including regions of large-scale separated flow. The skin-friction coefficient along the cylinder surface and its variation with Reynolds number are well captured in comparison with experiment. Proper separation behavior is observed.

Introduction

The flow of a Newtonian fluid over a cylinder is known to exhibit an interesting range of physical phenomena. With increasing $Re_D \equiv U_\infty D/\nu$, the flow develops from steady and stable with a closed wake, to two-dimensional and to three-dimensional flow following wake transition, shear-layer transition and possible boundary-layer transition. Beyond some critical Reynolds number Re_C (around $Re_D = 10^3$), the flow is observed to become turbulent owing to Kelvin-Helmholtz instability of the two shear layers that separate from the cylinder surface. The flow with $Re_D = 3900$ exceeds Re_C and is perhaps the most documented benchmark case in the literature. Some experimental studies at this Re_D focus on the character of the near-wall flow including Norberg [1], who documents pressure-coefficient measurements, while others, for example Lourenco & Shih [2] report results for mean velocity and turbulent intensity profiles in the near-wake region. In numerical simulation, Beaudan [3] first emphasized this specific case. Subsequent work by Kravchenko & Moin[4] and You & Moin [5], find a U-shape mean velocity profile inside the recirculation bubble rather than a V-shape profile as measured in experiment by Lourenco & Shih [2]. Ma et al. [6] discussed this contradiction by performing simulation using different span-wise domains. Their mean velocity converges to a U-shape when using $L_z = \pi D$, but to a V-shape for $L_z = 2\pi D$. Recently, Parnaudeau et al. [7] performed both experiments and numerical simulation that support the U-shape mean velocity profile. The issue remains an open question.

Above Re_C , the flow is typically characterized as having entered the subcritical regime where turbulence in the wake flow gets stronger and moves upstream with increasing Re_D . In this regime, some general tendencies can be observed for increasing Re_D , including increasing drag coefficient C_D and shrinking of the recirculation length. Weidman [8] studied the flow in this the subcritical Re_D range, finding that the pressure minima are similar from $Re_D = 10^4$ to 10^5 . There are however, limited numerical simulation results available in this regime that address the variation of the skin-friction C_f around the cylinder surface. This is expected to be important for understanding high Reynolds-number, bluff-body flows, where the near-wall velocity gradient increases with Re_D .

In the present study, we focus on the subcritical regime with the goal of providing detailed information on $C_f(\theta)$, where θ is the cylinder surface angle measured from the nominal forward

stagnation point, and on related flow-separation behavior.

Numerical method and physical models

The governing equations for the present LES are the formally filtered three-dimensional, incompressible Navier-Stokes equations:

$$\frac{\partial \tilde{u}_k}{\partial x_k} = 0 \quad (1)$$

$$\frac{\partial \tilde{u}_i}{\partial t} + \frac{\partial \tilde{u}_k \tilde{u}_i}{\partial x_k} = -\frac{\partial \tilde{p}}{\partial x_i} + \frac{1}{Re_D} \frac{\partial^2 \tilde{u}_i}{\partial x_k \partial x_k} - \frac{\partial T_{ki}}{\partial x_k} \quad (2)$$

in which T_{ik} is the unclosed stress tensor. In the present large-eddy simulation (LES), this is computed using the version of the stretched-vortex sub-grid stress model described by Chung & Pullin [9]. In the above equations, Cartesian coordinates (x, y, z) are used with corresponding velocity components (u, v, w) . In analyzing results, we also employ cylindrical coordinates (θ, y, r) , with $x = -r \cos \theta$, $z = r \sin \theta$ and with y the span-wise direction. Here $-\pi < \theta \leq \pi$ and the corresponding velocity components are (u_θ, u_y, u_r) .

The governing equations are spatially discretized in the computational domain on a collocated mesh, on which pressure-velocity coupling is achieved by the fractional step method [10]. In the predictor step, the convective and viscous terms are temporally discretized by two-step Adams-Bashforth and fully implicit schemes respectively. The pressure-Poisson equation on the curvilinear coordinate grid is solved by a multigrid solver with point- and line-relaxed Gauss-Seidel methods selectively chosen as solvers as well as smoothers. The energy conservative, fourth-order scheme, designed to conserve energy in discretization [11], is used. Parallelization is implemented using a standard MPI-protocol. To achieve near-optimal load balancing, the mesh is divided into blocks of equal size with each block assigned to a unique processor. All LES were performed on the Cray X86 supercomputer Shaheen at KAUST using up to 2048 cores.

In the present LES, we employ a standard O-grid. The mesh is stretched in the radial direction r , with minimum mesh size close to the cylinder surface. In the other azimuthal (θ) and span-wise (y) directions, the mesh is uniform. At the inlet, uniform flow $(u, v, w) = (U_\infty, 0, 0)$ is imposed while at the outlet plane, the convective outflow condition $\partial \mathbf{u} / \partial t + U_B \partial \mathbf{u} / \partial x = 0$ is used, in which U_B is the bulk velocity. No-slip boundary conditions are prescribed on the cylinder surface, and so the present simulation are considered wall-resolved LES. Periodic conditions are applied in the span-wise direction.

The stretched-vortex SGS model is based on the stretched-spiral vortex model Lundgren[12]. It assumes that in each computational cell, the subgrid motion is dominated by a vortex with direction \mathbf{e}^v , modeled by a delta-function probability density function (PDF). The tensor is given as [9]:

$$T_{ij} = (\delta_{ij} - \mathbf{e}_i^v \mathbf{e}_j^v) K, \quad K = \int_{k_c}^{\infty} E(k) dk = K_0' \Gamma[-1/3, \kappa_c^2] / 2 \quad (3)$$

Case	Re_D	N_θ	N_y	N_r	Δr_{min}
C0	3.9K	256	64	256	1.6×10^{-3}
F0	3.9K	384	96	384	1.2×10^{-3}
C1	10K	384	96	256	10^{-3}
C2	100K	768	192	384	3.7×10^{-4}

Table 1: LES performed. $K \equiv 10^3$. N_i is the mesh number in the ‘i’ direction.

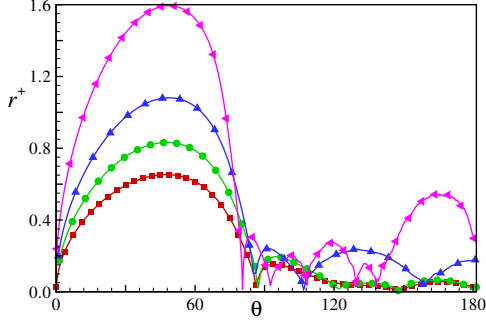


Figure 1: Δr^+ for the four cases. \bullet , C0; \blacksquare , F0; \blacktriangle , C1; \blacktriangledown , C2.

with $k_c = \pi/\Delta_c$ the cutoff wave-number and E the subgrid energy spectrum. In integration, Lundgren’s vortex model is used, with $K'_0 = K_0 \varepsilon^{2/3} \lambda_v^{2/3}$. Γ is the incomplete Gamma function with $\kappa_c = k_c \lambda_v$ and $\lambda_v = (2\nu/(3|\tilde{a}|))^{1/2}$. The rate-of-strain parameter $\tilde{a} = e_i^v e_j^j \tilde{S}_{ij}$ is the stretching along the subgrid vortex and $\tilde{S}_{ij} = (\partial \tilde{u}_i / \partial x_j + \partial \tilde{u}_j / \partial x_i) / 2$ is the resolved strain-rate tensor. By using a matching procedure, the composite parameter K'_0 can be found as $K'_0 = \langle F_2 \rangle / \langle Q(\kappa_c, d) \rangle$ where $\langle \cdot \rangle$ denotes a local average and is computed from a set of local points. The quantity F_2 is the local second-order structure function, calculated from the resolved-scale velocities while $Q(\kappa_c, d)$ is approximated using an asymptotic limit $\kappa_c \rightarrow 0$ with $d = r/\Delta_c$ and r the distance from a neighboring point to the vortex axis.

Cases and results

In the present LES, all cases employ the same domain: $L_y = 3D$ and $L_r = 40D$. Cases and corresponding meshes are listed in Table 1, which also shows the minimal mesh size in the wall normal direction. This is the size of the first mesh off the cylinder surface. In order to understand how well the present LES resolves the near-wall flow, a character parameter Δr^+ , which is the ratio of Δr_{min} to the wall unit length ν/u_τ , is plotted in figure 1.

Case 0: $Re=3900$

We compare the present LES with the experimental data of [7], the LES results of [3] and DNS results (case II) of [6]. The pressure coefficient C_p is shown in figure 2(a) where it can be seen that all results agree reasonably well. The relative difference between the present LES and the experimental data is roughly 3% at about 70° . The difference between coarse mesh case C0 and fine mesh case C1 is small. Additionally we compare $C_{f\theta}$ along the cylinder surface with experiment and DNS in figure 2(b) where

$$C_{f\theta} = \left. \frac{du_\theta}{dr} \right|_{r=0}, \quad (4)$$

and we note that presently, $C_{f\theta}$ is evaluated using only the radial derivative of u_θ , the velocity component along the tangential direction. We note that $C_{f\theta}$ at $Re = 3900$ is not directly measured

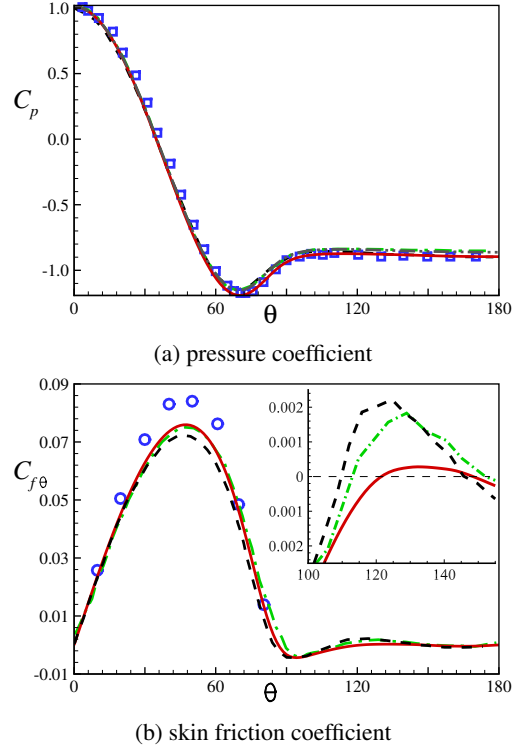
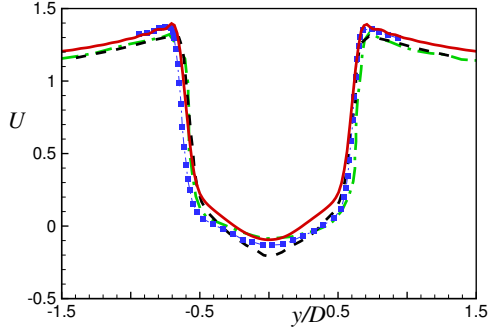


Figure 2: Comparison of pressure coefficient and skin friction coefficient. —, C0; — · —, F0; \square , experiments by [1]; \circ , experiments by [13]; — — —, LES by [3] — — — —, DNS by [6].

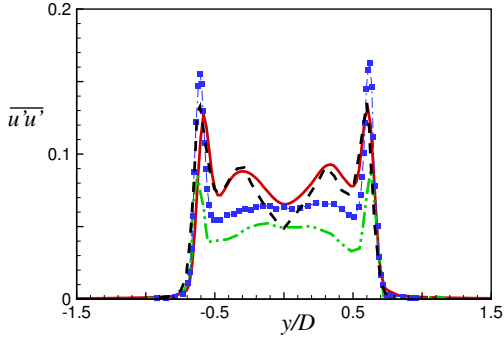
by Son & Hanratty [13]. Instead, in experiment they measured $C_{f\theta}$ at a series of cases with Re_D ranging from 5000 to 10^5 . Using this data they found that $C_{f\theta}$ at the front of the cylinder can be rescaled using $Re_D^{1/2}$. In other words, $C_{f\theta} Re_D^{1/2} = Const.$ Using this analogy, we have obtained an estimate of $C_{f\theta}$ at $Re = 3900$ from experiment results at $Re = 5000$.

The $C_{f\theta}$ distribution in present simulation shows good agreement with the above estimate except in the region around $\theta = 50^\circ$, where all simulation results are somewhat smaller than measurement. In the closeup inset of 2(b), we can see that all three simulations show a secondary separation bubble whose size and location differs for the three cases shown. Son & Hanratty [13] found that the separation angle for the secondary bubble decreases with increasing Reynolds number. At $Re_D = 5000$ it is about 120° . Extrapolating their results suggests a separation angle slightly larger than 120° at $Re = 3900$. In the present LES the separation of the secondary bubble, agrees well with this experiment, and takes place at an angle of 120° . This angle is definitely larger than 110° seen in other simulation results.

Although the issue of V-shape versus U-shape of the mean stream-wise velocity is still not resolved, we note that both the cited experiment and simulations with $L_z = \pi D$ find a U-shape profile. From figure 3(a), we can conclude that the differences between different simulation results and experiment are small and at approximately the same level. The present LES agrees quite well with the results of Kravchenko & Moin [4] except at around $y/D = 0$. Near the centerline $y/D = 0$, the present LES matches the valley value from experiments. In figure 3(b), we compare the stream-wise turbulent intensity $\overline{u'u'}$ profiles of experiment and numerical simulation. All simulation results deviate substantially from the measurements in the region $y/d \in (-0.5, 0.5)$. The present LES agree in the profile



(a) mean streamwise velocity .



(b) streamwise turbulent intensity.

Figure 3: Comparison of steamwise velocity and turbulent intensity. ■, experiments by [7]; —, C0; ---, LES by [4]; — · —, DNS by [6].

shape with the simulation result of Kravchenko & Moin [4].

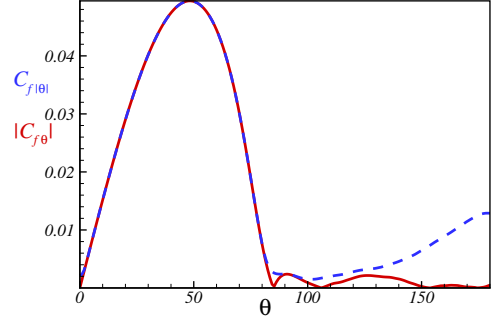
Subcritical regime: case 1 and case 2

LES for $Re = 10^4$ and 10^5 , as listed in the table were performed. Here we plot another measurement of skin-friction, which is defined based on the average of absolute value of velocity gradient along the θ direction:

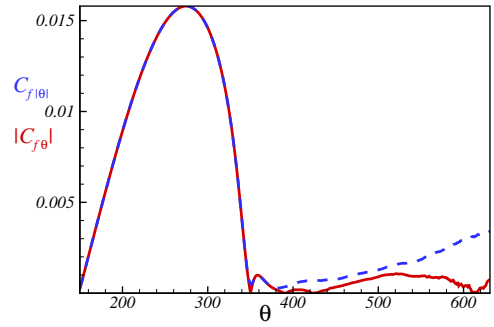
$$C_{f|\theta} = \frac{\overline{d|u_\theta|}}{dr} \Big|_{r=0} \quad (5)$$

This skin friction coefficient, will give values similar to $C_{f\theta}$ over the windward part of the cylinder surface where the flow is typically attached without reverse velocities, but rather different results near separation and in the well-separated region. This is because strong fluctuations in the separated flow region will affect $C_{f|\theta}$ but not $C_{f\theta}$. In Figure 4, we compare $C_{f|\theta}$ with $|C_{f\theta}|$ to show this difference. It can be seen that, for $Re_D = 10^4, 10^5$, $C_{f\theta}$ on that part of the cylinder surface where the flow has separated still shows reasonably small values, which are comparable to values for $Re_D = 3900$. In contrast, $C_{f|\theta}$ in the separated region shows a monotonically increasing tendency with increasing θ .

It is also of interest to examine an instantaneous field for skin-friction. In Figure 5, we compare instantaneous wall shear stress components $\tau_{w\theta}$ and τ_{wy} for the two Reynolds numbers. For both cases, we find that τ_{wy} is either very small or zero over the windward part of cylinder, which indicates small instantaneous span-wise velocities very near the wall. In the separated region, the fluctuation is quite strong. For $Re_D = 10^4$, the maximum fluctuation in τ_{wy} is of similar order to the maximum value for $\tau_{w\theta}$ over the front part of the cylinder while for $Re_D = 10^5$, the former is a factor of two times the latter.

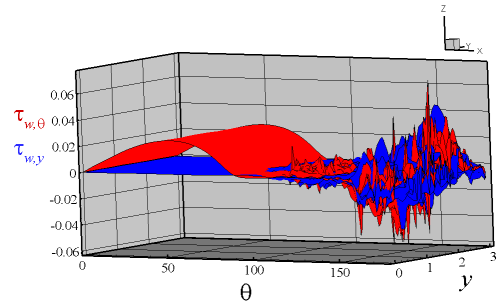


(a) $Re = 10^4$

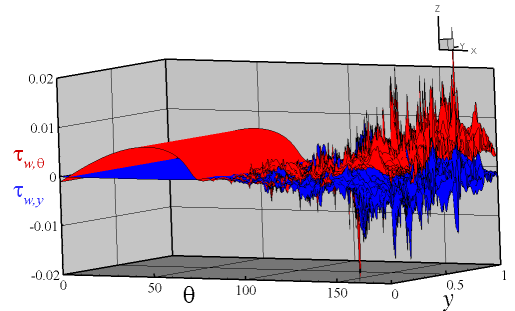


(b) $Re = 10^5$

Figure 4: Comparison of skin-friction coefficients: $C_{f|\theta}$ with $|C_{f\theta}|$.



(a) $Re = 10^4$



(b) $Re = 10^5$

Figure 5: Comparison of instantaneous wall shear stress.

Conclusions

In the present study, we describe an LES study of flow past a circular cylinder. For $Re_D = 3900$ some detailed comparisons with existing simulations and experiments are given, while for $Re = 10^4$ and $Re = 10^5$ the present LES give some indication of the effect of Re_D on flow properties. It is found that fluctuations of the instantaneous $C_{f\theta}$ in the separated region increase substantially with increasing Reynolds number while its time or span-wise average value remains reasonably small. It is also shown that $C_{f|\theta}$ can be a useful measurement of fluctuations in the skin friction coefficient. At large Re_D these fluctuations can be severe on the cylinder surface in the separated-flow region.

Acknowledgements

This work was supported partially by KAUST OCRF Award No. URF/1/1394-01 and partially by NSF award CBET 1235605 The Cray XC40, Shaheen, at KAUST was utilized for all the presently reported LES.

References

- [1] Norberg, N., Pressure Forces on a Circular Cylinder in Cross Flow, *IUTAM Symposium Bluff-Body Wakes, Dynamics and Instabilities*, 1993
- [2] Lourenco, L.M. and Shih, C., Characteristics of the plane turbulent near wake of a circular cylinder, a particle image velocimetry study, *Stanford University*, TF-62, 1994
- [3] Beaudan, P. and Moin, P., Numerical experiments on the flow past a circular cylinder at sub-critical Reynolds number *Stanford University*, TF-62, 1994
- [4] Kravchenko, A. G. and Moin, P., Numerical studies of flow over a circular cylinder at $Re_D = 3900$, *Physics of Fluids*, 12, 403-417, 2000
- [5] You, D. and Moin, P., A dynamical global-coefficient subgrid-scale eddy-viscosity model for large-eddy simulation in complex geometries, *Physics of Fluids*, 19, 065110, 2007
- [6] Ma, X., Karamanos, G.S., and Karniadakis G.E., Dynamics and low-dimensionality of a turbulent near wake, *Journal of Fluid Mechanics*, 410, 29-65, 2000.
- [7] Parnaudeau, P., Carlier, J., Heitz D and H. Lamballais, Experimental and numerical studies of the flow over a circular cylinder at Reynolds number 3900 *Physics of Fluids*, 20, 085101, 2008.
- [8] Weidman, P., Wave Transition and Blockage Effects on Cylinder Base Pressure, *California Institute of Technology*, 1968
- [9] Chung D., and Pullin D.I., Large-eddy simulation and wall modeling of turbulent channel flow, *Journal of Fluid Mechanics*, 631, 281-309, 2009
- [10] Zang, Y., Street, R.L. and Koseff J.R., A Non-staggered Grid, Fractional Step Method for Time-Dependent Incompressible Navier-Stokes Equations in Curvilinear Coordinates, *Journal of Computational Physics*, 114, 18-33, 1994
- [11] Morinishi Y., Lund T.S., Vasilyev O.V. and Moin P., Fully conservative higher order finite difference schemes for incompressible flow, *Journal of Computational Physics*, 143, 90-124, 1998
- [12] Lundgren, T.S., Strained spiral vortex model for turbulent fine structure, *Physics of Fluids*, 25, 2193-2203, 1982
- [13] Son, J.S. and Hanratty T.J., Velocity gradients at the wall for flow around a cylinder at Reynolds numbers from 5×10^3 to 10^5 , *Journal of Fluid Mechanics*, 35:353-368, 1969